Journal of Neurochemistry

JOURNAL OF NEUROCHEMISTRY | 2015 | 135 | 616–629 doi: 10.1111/jnc.13288

ORIGINAL ARTICLE

Cannabinoid receptor type 1 agonist ACEA improves motor recovery and protects neurons in ischemic stroke in mice

Laura Caltana, Trinidad Maria Saez, María Paula Aronne and Alicia Brusco

Instituto de Biología Celular y Neurociencia "Prof. E. De Robertis" (UBA-CONICET). Facultad de Medicina, Universidad de Buenos Aires, Ciudad Autónoma de Buenos Aires, Argentina

Abstract

Brain ischemia produces neuronal cell death and the recruitment of pro-inflammatory cells. In turn, the search for neuroprotection against this type of insult has rendered results involving a beneficial role of endocannabinoid receptor agonists in the Central Nervous System. In this work, to further elucidate the mechanisms associated to this neuroprotective effect, focal brain ischemia was generated by middle cerebral artery occlusion (MCAo) in C57Bl/6 mice. Three, 24 and 48 h after MCAo, animals received CB1R agonist ACEA (1 mg/kg), CB1R antagonist AM251 (1 mg/kg) or vehicle. To assess motor activity, neural deficit scores and motor tests were performed 1 day before and 3, 7, 14, 21, and 28 days after MCAo. At 7 and 28 days post lesion, cytoskeleton structure, astroglial and microglial reaction, and alterations in synapsis were studied in the cerebral cortex. ACEA treatment reduced astrocytic reaction, neuronal death, and dendritic loss. In contrast, AM251 treatment increased these parameters. Motor tests showed a progressive deterioration in motor activity in ischemic animals, which only ACEA treatment was able to counteract. Our results suggest that CB1R may be involved in neuronal survival and in the regulation of neuroprotection during focal cerebral ischemia in mice.

Keywords: cannabinoid receptor agonist, Cerebral ischemia, neuronal death, neuroprotection.

J. Neurochem. (2015) **135**, 616–629.

Stroke ranks as the fourth cause of death and one of the leading causes of long-term disability (American Heart Association Statistics Committee and Stroke, 2014). It is soon followed by inflammation, with microglia and mast cells acting as early responders (Silver and Curley 2013), whereas additional late-phase responses include reactive astrocytosis and the resulting glial scar formation in the boundary zone of the ischemic core, which plays a critical role and may have beneficial or detrimental effects (Sofroniew and Vinters 2010).

The endocannabinoid system consists of lipid-based mediators, endocannabinoids (eCB), their target receptors, associated synthesizing and metabolizing enzymes and transporter proteins. Cannabinoid receptor type 1 (CB1R) is expressed in neurons and glial cells in many brain regions, where it plays neuromodulatory roles in brain function (Sánchez-Blázquez *et al.* 2014), whereas Cannabinoid receptor type 2 (CB2R) is mainly expressed by cells of the immune system. eCB act as retrograde messengers and regulate synaptic transmission through pre-synaptic CB1R. They have also been identified as triggers for short- and long-term plasticity at synapses throughout the brain (Heifets and Castillo 2009).

Cannabinoids (including eCB, phytocannabinoids, and synthetic compounds) could reduce the effects of diverse pathologies in liver, heart and also protect the brain against hypoxia/ischemia (Pacher and Hasko 2008), although the molecular mechanisms are still unclear. Evidence suggests that eCB signaling can regulate excitotoxicity by reducing glutamate release (Parmentier-Batteur *et al.* 2002).

In this context, the aim of this work was to evaluate eCB potential effects in a mouse model of permanent middle cerebral artery occlusion (MCAo) by analyzing motor

Received November 7, 2014; revised manuscript received August 4, 2015; accepted August 15, 2015.

Address correspondence and reprint requests to Laura Romina Caltana, Paraguay 2155, 3rd floor, Instituto de Biologia Celular y Neurociencia, Facultad de Medicina, Universidad de Buenos Aires. Ciudad Autónoma de Buenos Aires (1121), Argentina. E-mail: lauracaltana@gmail.com

Abbreviations used: MCAo, middle cerebral artery occlusion; ROD, relative optical density; TEM, transmission electron microscope.

activity, neuronal degeneration, and astrocytic and microglial reactions before and after the ischemic event.

Materials and methods

Animals

Adult male C57/Bl6 mice (25–32 g) obtained from the Animal Facility at the National Center of Atomic Energy were used in this study. Sixty mice were housed in a humidity- and temperature-controlled environment (12 h/12 h light/dark cycle), with free access to food and water. Animal treatments were in accordance with CICUAL protocols (Institutional Committee for the Care and Use of Laboratory Animals, School of Medicine, University of Buenos Aires).

Mouse model of middle cerebral artery occlusion (MCAo)

Mice were deeply anesthetized with an intraperitoneal (i.p.) dose of ketamine/xylazine (100 μg/g 10 μg/g in 10 μL saline) and the MCA was exposed and permanently occluded by electrocoagulation (Wagner *et al.* 2011, modified for mice). Sham procedure was performed as described above except for coagulation of the MCA. Animal survival rate was 100%.

Cannabinoid agonist/antagonist treatment

Adult mice were randomly assigned to six groups (n = 10 in each group) per recovery time (3, 24, and 48 h after surgical procedure) and i.p. injected CB1R agonist ACEA (arachidonyl-2-chloroethylamide) 1 mg/kg (García-Arencibia *et al.* 2007) or CB1R antagonist AM251 1 mg/kg (Price *et al.* 2009). Both drugs were first dissolved in dimethylsulfoxide and diluted in saline. The control groups were injected the same volume of dimethylsulfoxide dissolved in saline solution at the same time points.

Behavioral tests: motor activity

Neurological score

Neurological examinations were performed on Day 1 (D1) 3 h after surgical procedure, D2–D4, D7, D14, D21, and D28 (Longa *et al.* 1989). The neurological findings were scored on a five-point scale: 0-no neurological deficit, 1-failure to fully extend left forepaw, 2-circling to the left, 3-falling to the left, 4-no spontaneous walking, and a depressed level of consciousness.

Corner and cylinder tests

Motor activity tests were performed according previous studies, for corner test details see Zhang *et al.* 2002 and for cylinder test Li *et al.* 2004 and Schallert *et al.* 2000).

Morphological analysis

After 7- to 28-day recovery (D7 and D28), five animals in each group were fixed by intracardiac perfusion with 4% (w/v) paraformaldehyde in 0.1 M phosphate buffer (PB), pH 7.4, and coronal sections of the brains were cut with a vibratome (25 μm).

Toluidine blue staining

Brain sections were rinsed with phosphate-buffered saline and then incubated in toluidine blue 0.5% (w/v) dissolved in sodium carbonate 2.5% (w/v).

Fluoro-Jade® B staining procedure

Brain sections mounted onto gelatin-coated slides were stained with Fluoro-Jade® B (Millipore, Temecula, CA, USA) (Balan *et al.* 2006).

Immunohistochemical staining

Immunohistochemistry was performed with primary antibodies: rabbit anti-glial fibrillary acidic protein (GFAP, 1 : 3000, Dako, Carpinteria, CA, USA); mouse anti-synaptophysin (Syn, 1 : 1000; Sigma, St Louis, MO, USA); mouse anti-microtubule-associated protein type2 (MAP-2, 1 : 1000, Sigma); rabbit anti-CB1R (1 : 5000, Cayman Chemical, Ann Arbor, MI, USA); rabbit anti-vesicular transporter glutamate (VGlut1, 1 : 2000, Santa Cruz Biotechnology, Santa Cruz, CA, USA); rabbit anti-subunit 4 of α-amino-3-hydroxy-5-methylisoxazole-4-propionate receptors (GluR4, 1 : 1000, Cell Signaling Technology, Beverly, MA, USA), mouse anti-SMI311 (PAN, 1 : 4000, Abcam, Cambridge, MA, USA). For immunofluorescent labeling, after incubation with primary antibodies, brain sections were washed in phosphate-buffered saline and incubated for 4 h with fluorescent secondary antibodies anti-mouse, anti-guinea pig and anti-rabbit IgG conjugated with FITC or Texas Red (1 : 500, Vector Laboratories, Burlingame, CA, USA) (Caltana *et al.* 2009). Sections were later counter-stained with Hoechst 33342 (2 μg/mL, Sigma).

Lectin staining

Brain sections were incubated for 48 h at 4°C with the biotinylated lectin *Lycopersicon esculentum lectin* (6 μg/mL, Sigma) (for details, see Caltana *et al.* 2009).

Ultrastructural analysis

A set of 12 animals (2 per group) was fixed by intracardiac perfusion with 4% (w/v) paraformaldehyde and 0.25% (v/v) glutaraldehyde in PB at D7, and tissue was then processed for electron microscopy. Images were acquired on a *Zeiss 109* transmission electron microscope (TEM) (Carl Zeiss, Oberkochen, Germany) and photographed with a GATAN CCD camera (Pleasanton, CA, USA). For TEM images, the synapse number per 100 μm^2 was measured.

Morphometric digital image analysis

Images were acquired on an *Axiolab* epifluorescence microscope (Carl Zeiss) equipped with a Q-Color3 CCD camera (Olympus, Tokyo, Japan). Counting and morphometry were performed using Image Pro PLUS 4.5 (Media Cybernetics, Warrendale, PA, USA) and Image J (NIH, http://rsb.info.nih.gov/ij/) software.

The brain area analyzed was the primary motor cortex (M1/M2) (Franklin and Paxinos 2007). In each coronal section, each microscopic field was selected within the limits of the penumbra ischemic area and morphometrically analyzed. The intensity of Syn, VGlut1, and Glur4 immunoreactivity (ir) was evaluated by means of a relative optical density (ROD) value as previously described (Evrard *et al.* 2006). Color images were randomly acquired and then transferred to black and white images (Jung *et al.* 2009).

Lectin$^+$ and Fluorojade B$^+$ cells were quantified. For astrocyte GFAP-ir, the cell area was evaluated by interactively determining each cell limit. To evaluate CB1R-ir, MAP-2-ir, and PAN fibers, the total area of the immunolabeled fibers was related to the total area of the corresponding microscopic field (20× primary magnification), rendering a relative area parameter.

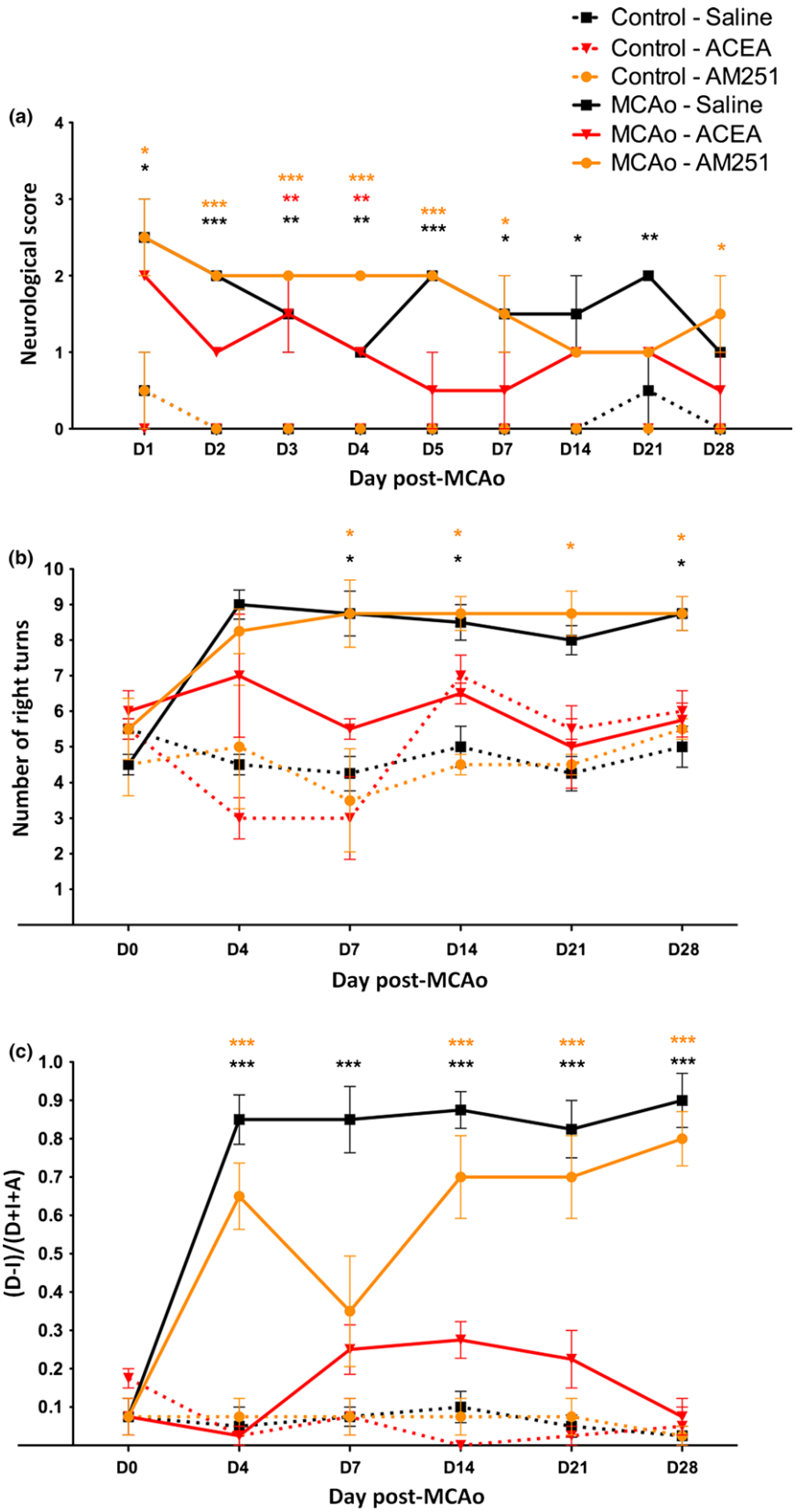

Fig. 1 (a) Evolution of neurological scores during treatment. (b) Corner test. (c) Cylinder test. Significance between treatments after one-way ANOVA and Dunnet post-test $*p < 0.05$; $**p < 0.01$; $***p < 0.001$. Comparisons were done to Control-Saline groups. Asterisk colors correspond to: Black-MCAo-Saline group; Red-MCAo-ACEA group; Yellow-MCAo-AM251 group. $n = 10$ per group.

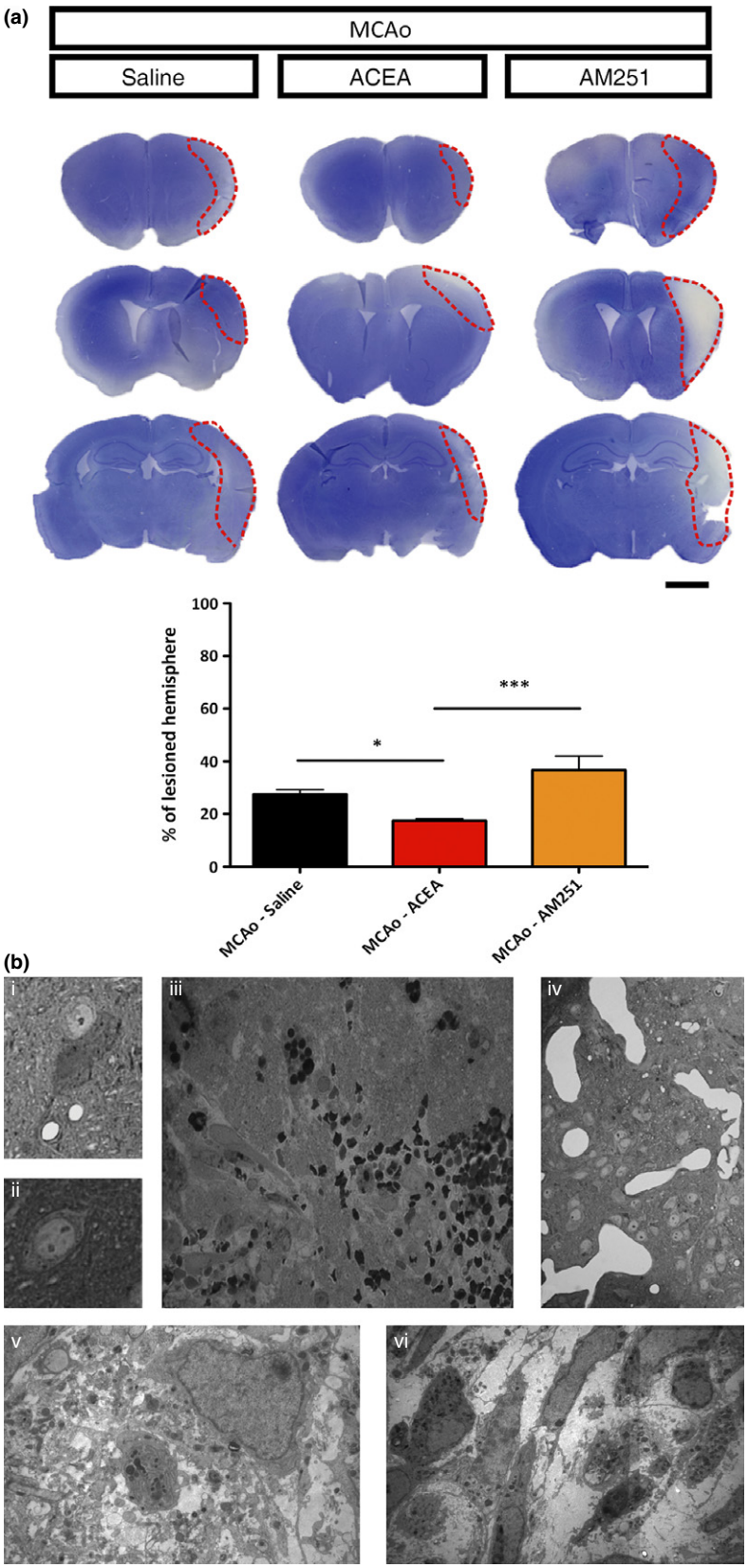

Fig. 2 (a) Brain slices showing infarct area and percentage of injured hemisphere. Significance between treatments after one-way ANOVA and Tukey post-test $*p < 0.05$; $***p < 0.001$. (b) (i). Degenerated neurons. (ii) Normal neurons. (iii) Inflammatory infiltrate. (iv) Angiogenesis. (v) and (vi) Extracellular edema. Scale bar: (i) and (ii): 10 μm, (iii) and (iv): 50 μm, (v): 1 μm and F: 2 μm.

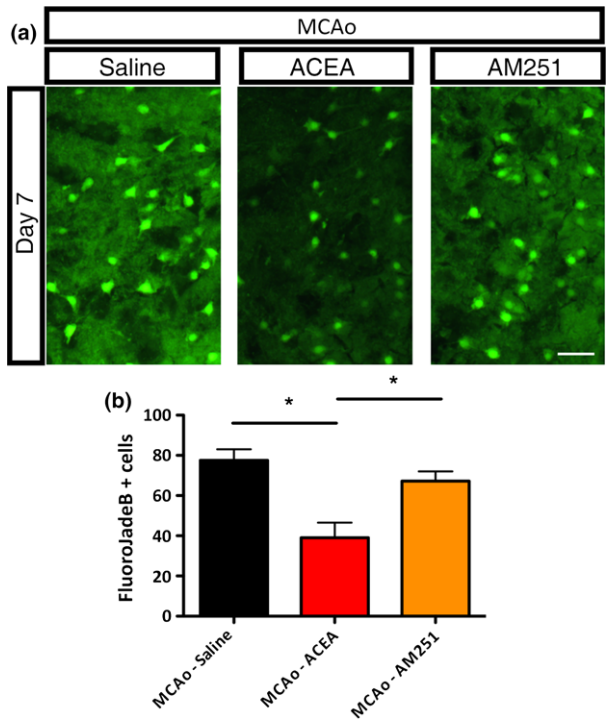

Fig. 3 (a) Fluorojade-B staining in the ischemic penumbra. (b) Number of Fluorojade B^+ cells after treatment. Significance between treatments after one-way ANOVA and Tukey post-test. *$p < 0.05$. Scale bar: 30 μm.

The ischemic area was estimated as a fraction of the total contralateral hemisphere.

Statistical analysis

Reported values represent the mean ± SEM of experiments performed for each marker. Differences among the means of the six groups were statistically analyzed by one-way analysis of variance (ANOVA), followed by Tukey's test (for morphological analysis) or Dunnet's test (for motor activity tests), $p < 0.05$, using GraphPad Prism v5.00 software (GraphPad Software Inc., San Diego, CA, USA). To simplify graphic presentation, values of the different groups are expressed as percentages of the sham-operated saline-treated group (Control-Saline) (value = 100%).

Results

CB1R agonist ACEA facilitated motor activity recovery

During the first 4 days after MCAo, ischemic mice exhibited significantly elevated neurological deficit scores compared to the control groups. From D7 to D28, MCAo-Saline and MCAo-AM251 groups showed an elevated score, which persisted until D21 and D28. The MCAo-ACEA group showed a reduction in neurological deficit scores since D5 (Fig. 1a). All experimental groups were evaluated prior to MCAo in the corner and cylinder tests to assess basal parameters.

At D0, none of the groups showed behavioral asymmetries in the corner test (similar number of turns toward either side). Control and MCAo-ACEA groups maintained the same tendency during the experimental period, whereas the other MCAo groups showed a significant increase in right turns compared with Control-Saline. MCAo-Saline and MCAo-AM251 showed an elevated number of right turns until D28 (Fig. 1b).

Meanwhile, in the cylinder test, all groups showed similar scores at D0 and Control groups did not show differences after surgery. After MCAo, the MCAo-Saline and MCAo-AM251 groups showed a significant increase in cylinder test scores, reflecting asymmetrical behavior. The MCAo-ACEA group did not show differences with Control-Saline (Fig. 1c).

CB1R agonist ACEA reduced infarct area size and neuronal degeneration

Brain sections were stained with toluidine blue to measure lesion size. Control groups did not show any evidence of lesion at D28 post surgery (data not shown). After MCAo, MCAo-Saline showed a reduction in lesion size after ACEA treatment and an increase with AM251 administration (Fig. 2).

To determine whether the improvement in motor activity and the reduction in infarct size were related with decreased neuronal damage, Fluoro-Jade B was used to stain cell bodies, dendrites, axons, and axon terminals of degenerating neurons and Fluoro-Jade B^+ cells were analyzed in the penumbra cortex, surrounding the ischemic core. At D7, there were no Fluoro-Jade B^+ cells in the control groups (data not shown) but, in the MCAo groups (Fig. 3a), the number of Fluoro-Jade B^+ neurons in the cortex was significantly higher in the Saline- and AM251-treated animals than in ACEA-treated ones, which shows the protective effects of CB1R stimulation against neuronal degeneration after ischemic insult (Fig. 3b).

CB1R agonist ACEA reduced astroglial reaction after MCAo

Astrocytic reaction was evaluated by measuring the area occupied by $GFAP^+$ astrocytes. No changes were observed in the cerebral cortex in astrocytic cell area, astrocytic shape or their organization pattern in any of the control groups. Astrocyte cell area increased after MCAo at D7 and D28 and did not change in the AM251-treated group (Fig. 4a). Treatment with ACEA induced a reduction in astroglial reaction. Indeed, astrocytes showed normal shape with thinner and shorter projections at D7 and D28 as compared to MCAo-Saline and MCAo-AM251 (Fig. 4b and c).

CB1R agonist ACEA reduced microglial response after MCAo

The level of microglial activation was assessed by determining the number of $lectin^+$ cells with stellate and ameboid

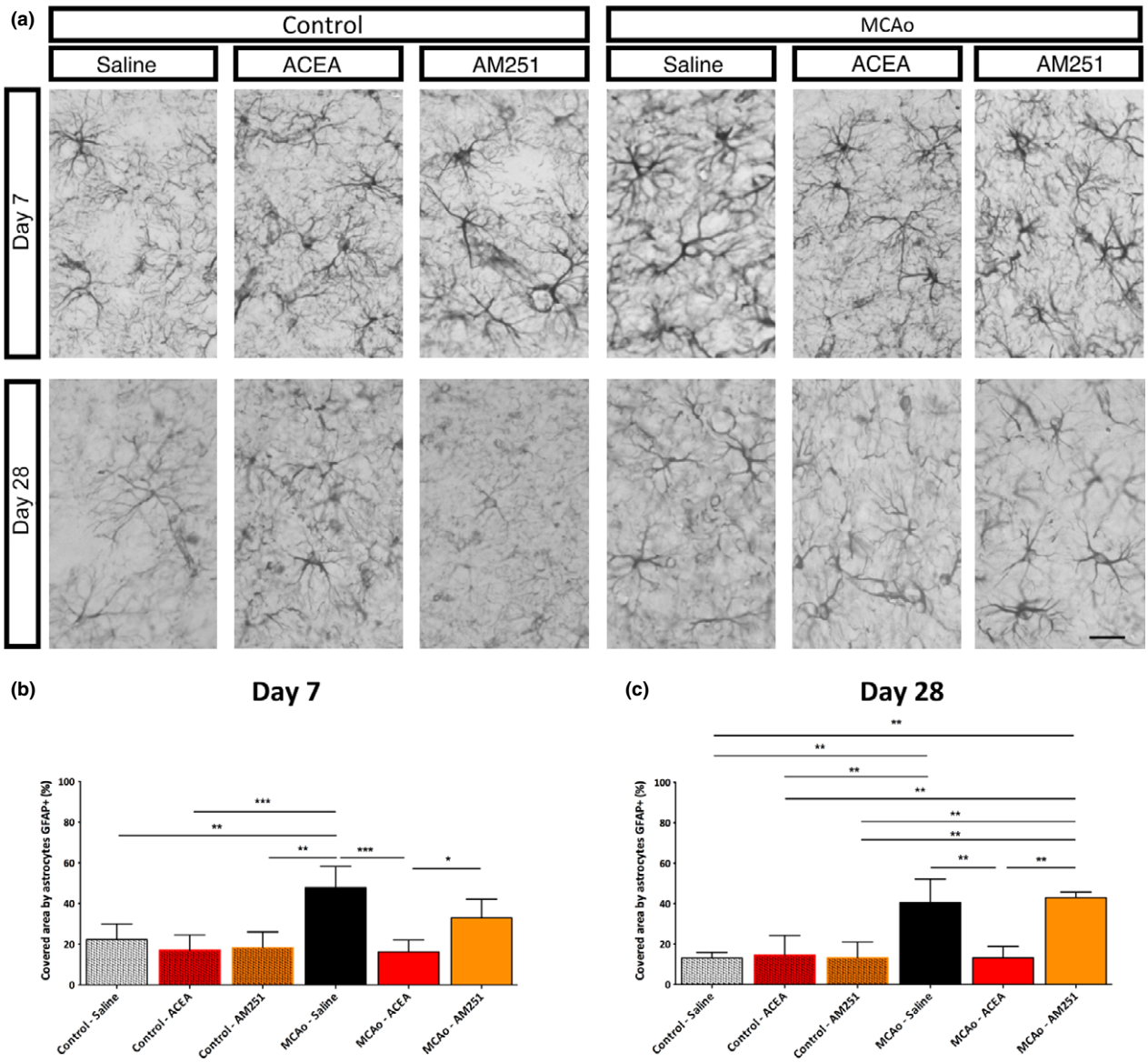

Fig. 4 (a) GFAP immunostaining. (b and c) Area covered by GFAP$^+$ astrocytes at D7 and D28, respectively. Significance between treatments after one-way ANOVA and Tukey post-test $*p < 0.05$; $**p < 0.01$; $***p < 0.001$. Scale bar: 30 μm.

shape. There were no differences across Control groups in the number of lectin$^+$ cells (stellate or ameboid) and microglial cells were typically ramified with multiple branches (Fig. 5a). A robust microglial response was observed after MCAo because of a significant increase in the number of lectin$^+$ cells (Fig. 5b and c). Moreover, changes were detected in cell shape (becoming ameboid and round). The ACEA-treated group presented lower microglial activation compared with Saline- or AM251- treated groups in relation with the number of stellate and ameboide lectin$^+$ cells at D7 (Fig. 5b) and ameboid lectin$^+$ cells at D28 (Fig. 5c).

CB1R stimulation modified the effects of ischemia on neuronal cytoskeleton

MAP2 is a microtubule-associated protein present in neuronal dendritic processes, commonly used to analyze the dendritic tree and its extension. MCAo produced a significant reduction in the relative area covered by the MAP2-ir dendrites (Fig. 6), which recovered with ACEA treatment at D7 and D28. The MCAo-ACEA group displayed an increase in the area covered by MAP2-ir dendrites, mainly because of enhanced length, branching, and thickness; the area covered by MAP2$^+$ fibers did not show different values to those observed in the control

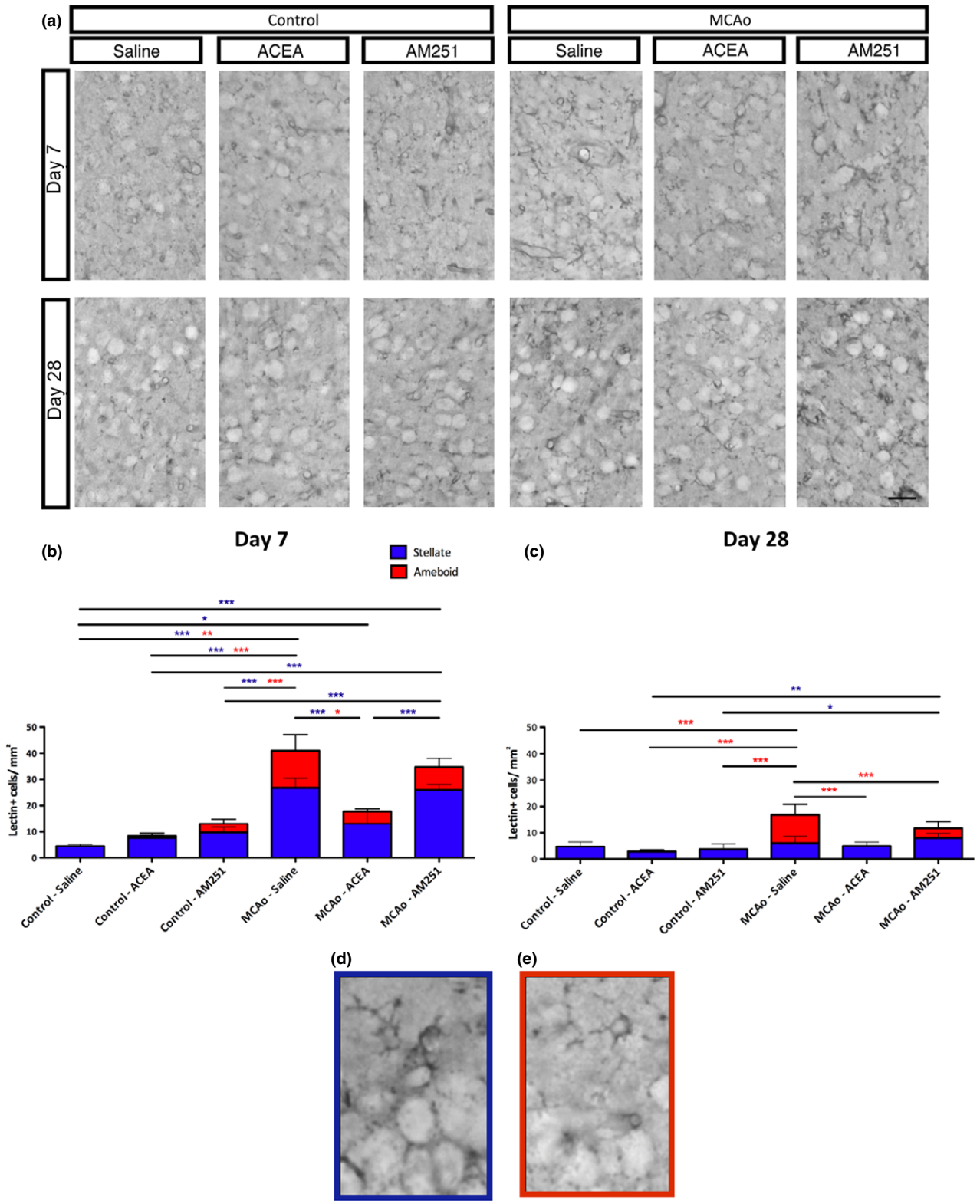

Fig. 5 (a) Lectin immunostaining. (b and c) Number of lectin$^+$ cells at D7 and D28, respectively. Bars in blue and red represent stellate cell shape and ameboid cell shape counting, respectively. (d) Representative stellate microglial cell. (e) Representative ameboid microglial cell. Significance between treatments after one-way ANOVA and Tukey post-test $*p < 0.05$; $**p < 0.01$; $***p < 0.001$. Scale bar: 30 μm.

groups. The dendrite area obtained in MCAo groups treated with Saline or AM251 did not present differences (Fig. 6b and c).

PAN immunostaining was used to label total neurofilaments, the main determinant factor in axonal diameter. At D28, the area covered by PAN$^+$ fibers in control groups showed thin and regular PAN-immunostained fibers (Fig. 7a and 7b). MCAo groups treated with Saline or AM251 showed changes in the morphology of PAN$^+$ fibers – thicker, irregular and wavy (Fig. 7b) – and a decrease in the tissue area covered by these PAN$^+$ fibers. The MCAo-ACEA group showed no changes in PAN$^+$ fiber pattern, presenting features similar to the control, but with an increase in the area covered (Fig. 7b).

CB1R agonist ACEA modified CB1R expression after MCAo

The expression of CB1R was assessed by measuring the area covered by CB1R-ir fibers. In control groups, no changes in CB1R expression were observed. After MCAo, ACEA treatment increased CB1R expression, whereas the MCAo-AM251 group showed a decrease in this parameter (Fig. 8a and b).

MCAo produced changes at synaptic level

Electron microscopy was used to assess the number of synapses, calculated per 100 μm^2 in the penumbra. MCAo reduced the number of synapses, probably because of neuronal death and tissue damage. After ACEA treatment, the number of synapses increased compared to

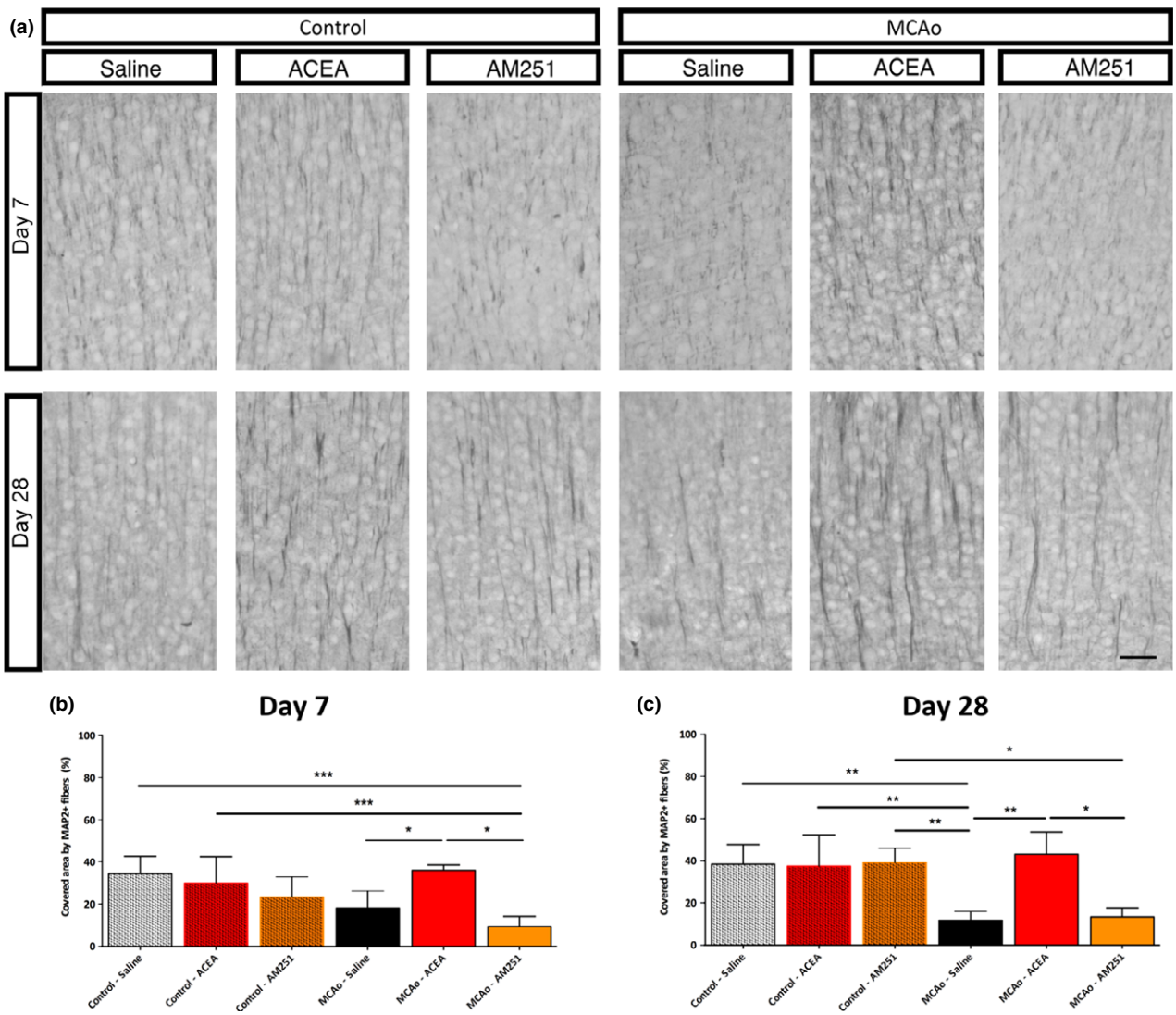

Fig. 6 (a) MAP2 immunostaining. (b) Area covered by MAP2$^+$ fibers at D7. (c) Area covered by MAP2 + fibers at D28. Significance between treatments after one-way ANOVA and Tukey post-test $*p < 0.05$; $**p < 0.01$; $***p < 0.001$. Scale bar: 30 μm.

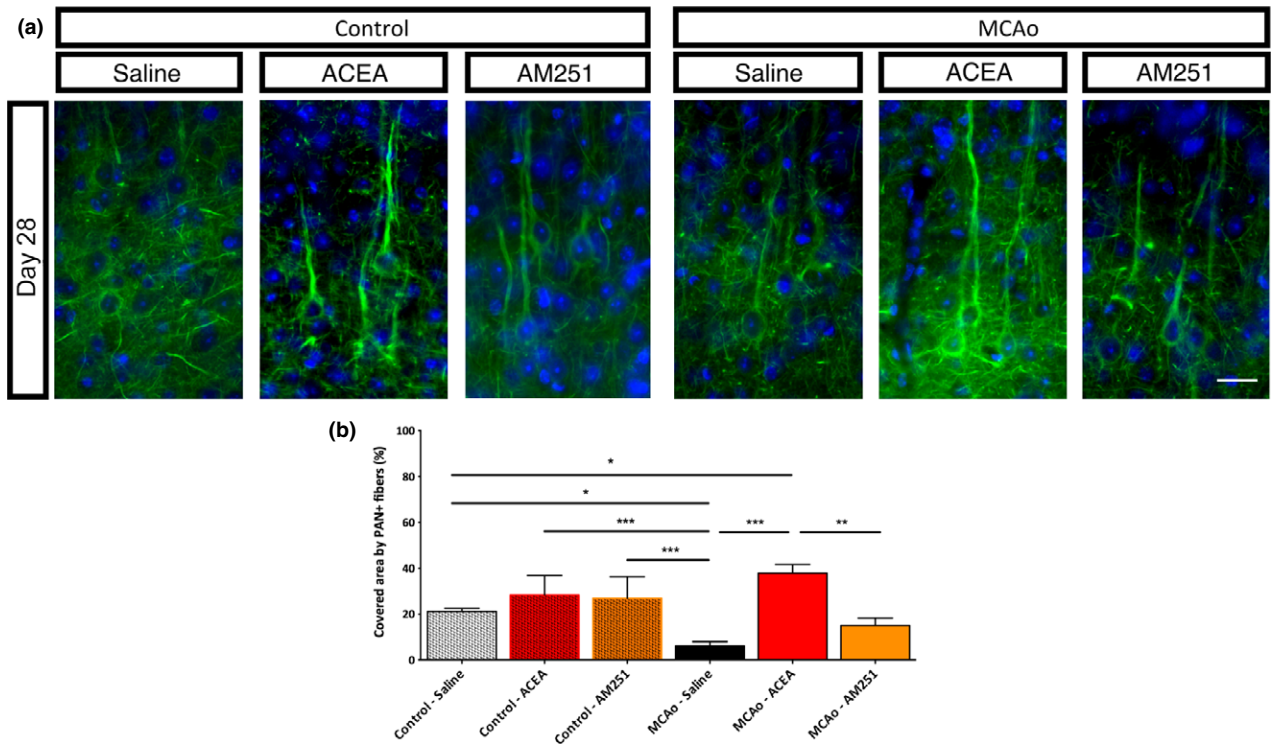

Fig. 7 (a) PAN immunostaining. (b) Area covered by PAN$^+$ fibers at D28. Significance between treatments after one-way ANOVA and Tukey *post-test* $*p < 0.05$; $**p < 0.01$; $***p < 0.001$. Scale bar: 30 μm.

Control, MCAo-Saline and MCAo-AM251 groups (Fig. 9a and b).

For Syn, Vglut1, and GluR4 ROD measurements, color images were acquired randomly in the cerebral cortex and then transferred to black and white images. The data were transformed to percentages, considering Control-Saline groups as 100%.

Syn is a specific marker for pre-synaptic boutons and is also considered a marker for synaptogenesis. Exposure to CB1R agonists or antagonists did not produce significant changes in Syn ROD in control groups; after MCAo, Syn ROD increased only in the MCAo-Saline group, whereas MCAo-ACEA and MCAo-AM251 showed no differences with respect to the Control-Saline group (Fig. 10a and b), which suggests that CB1R stimulation reduces synaptogenesis.

Glutamate is the most abundant excitatory neurotransmitter in the CNS and it is packaged in vesicles for later release during synaptic transmission. These vesicles contain Vglut1, which is expressed in the adult brain. It has been proposed that Vglut1 levels are critical to the balance between excitatory and inhibitory transmission (Todd *et al.* 2003). The expression of Vglut1 increased in MCAo-Saline and MCAo-AM251 groups with respect to the control group, but decreased in the MCAo-ACEA group (Fig. 10a and c), changes which could be related to modifications in the synthesis or release of glutamate.

The α-amino-3-hydroxy-5-methylisoxazole-4-propionate receptors are ionotropic glutamate transmembrane receptors formed by four types of subunits (GluR1, GluR2, GluR3, and GluR4) which mediate rapid synaptic transmission in the CNS (Mayer 2011). The expression of ionotropic glutamate receptor type 4 was analyzed and no changes were observed in GluR4 ROD, either in Control or MCAo groups (Fig. 10a and d).

Discussion

The eCB signaling system, integrated by its ligands, membrane receptors and regulatory proteins, has been described as a potential therapeutic target for obesity, drug abuse, pain, and stroke. Moreover, cannabinoid agonists have become potentially attractive neuroprotective agents in medical research.

CB1 agonists, like WIN-55212-2, ACEA, HU210, THC, and AM404, have presented potential neuroprotective effects (Docagne *et al.* 2007; García-Arencibia *et al.* 2007; Zani *et al.* 2007) and are useful in the treatment of neuronal disorders, acting through the inhibition of excitotoxicity, cell death, inflammation, and oxidative stress (Vendel and de Lange 2014). In particular, ACEA is a cannabinoid agonist with neuroprotective properties in different animal models of CNS injury (Bahremand *et al.* 2009). In this context, this

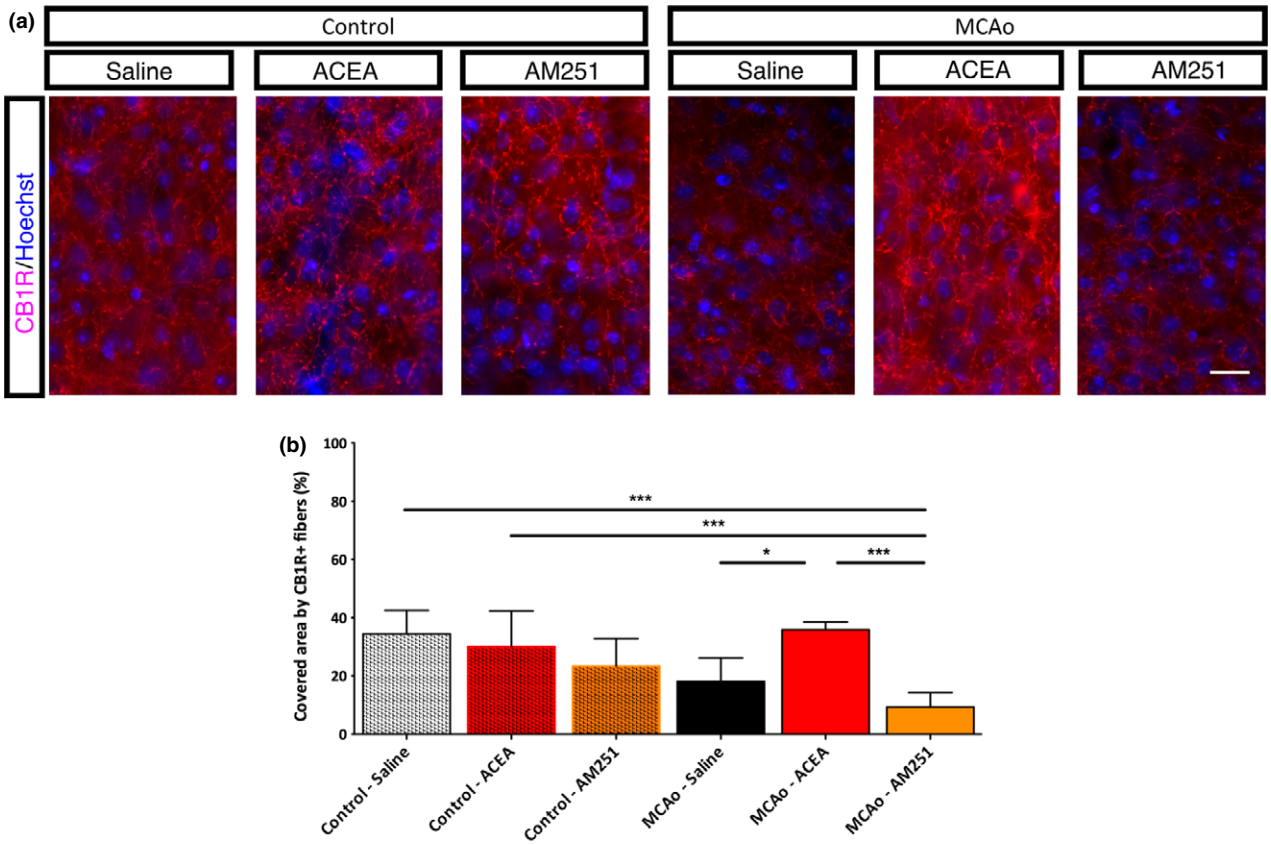

Fig. 8 (a) CB1R immunostaining. (b) Area covered by CB1R$^+$ fibers at D7. Significance between treatments after one-way ANOVA and Tukey post-test $*p < 0.05$; $***p < 0.001$. Scale bar: 30 μm.

study was designed to further ascertain the neuroprotective properties of this CB1 agonist following ischemic stroke in a model of MCAo in mice. The treatment scheme was designed to avoid undesirable effects and the doses used were lower than those producing psychotropic effects.

We show here that ACEA protected brain regions affected by ischemia and ameliorated the deterioration of motor activity after MCAo, reducing asymmetric motor alterations and spontaneous activity. ACEA also reduced neuronal degeneration and death, dendrite loss, and microglial reaction. These findings are in agreement with previous reports where a variable level of neuroprotection was induced by CB agonists (Mauler *et al.* 2003; Youssef *et al.* 2007).

We also show important changes in the neuronal cytoskeleton following MCAo. We found a decrease in the relative area covered by neuronal processes in the cerebral cortex, probably indicating a reorganization of the cytoskeletal structure related with neuronal suffering. MAP2-immunostained dendrites from the cortical area (M1/M2) were thicker and presented an irregular structure, whereas the MAP2$^+$ relative area was reduced. After ACEA treatment, this relative area increased to reach control levels, probably reflecting an increased dendrite thickness and/or increased branching, characteristic of sprouting phenomena. CB1R antagonist AM251 did not produce alterations in the Control groups, whereas the MCAo group showed a decrease in dendritic arborization after ischemic insult which had not recovered by D28. Results obtained in PAN immunostaining showed that MCAo induced a decrease in the area covered by neurofilaments, a parameter which recovered after ACEA treatment.

Neuronal differentiation, synapse formation and the preservation of tissue microenvironment in nervous tissue are regulated by astrocytes (Wang and Bordey 2008). Reactive astrogliosis consists of morphological changes including an increase in cell size with thicker and longer cellular processes related with alterations in cytoskeletal proteins, specifically GFAP. In our studies, MCAo was observed to produce astrocytic reaction at D7, characterized by an increase in the number of astrocytes and cell area in cortex which persisted at D28, but was reversed by ACEA treatment.

Cerebral ischemia induces an inflammatory reaction with activation of astrocytes and microglial cells. Damaged tissue releases different cytokines and neurotransmitters and acts on

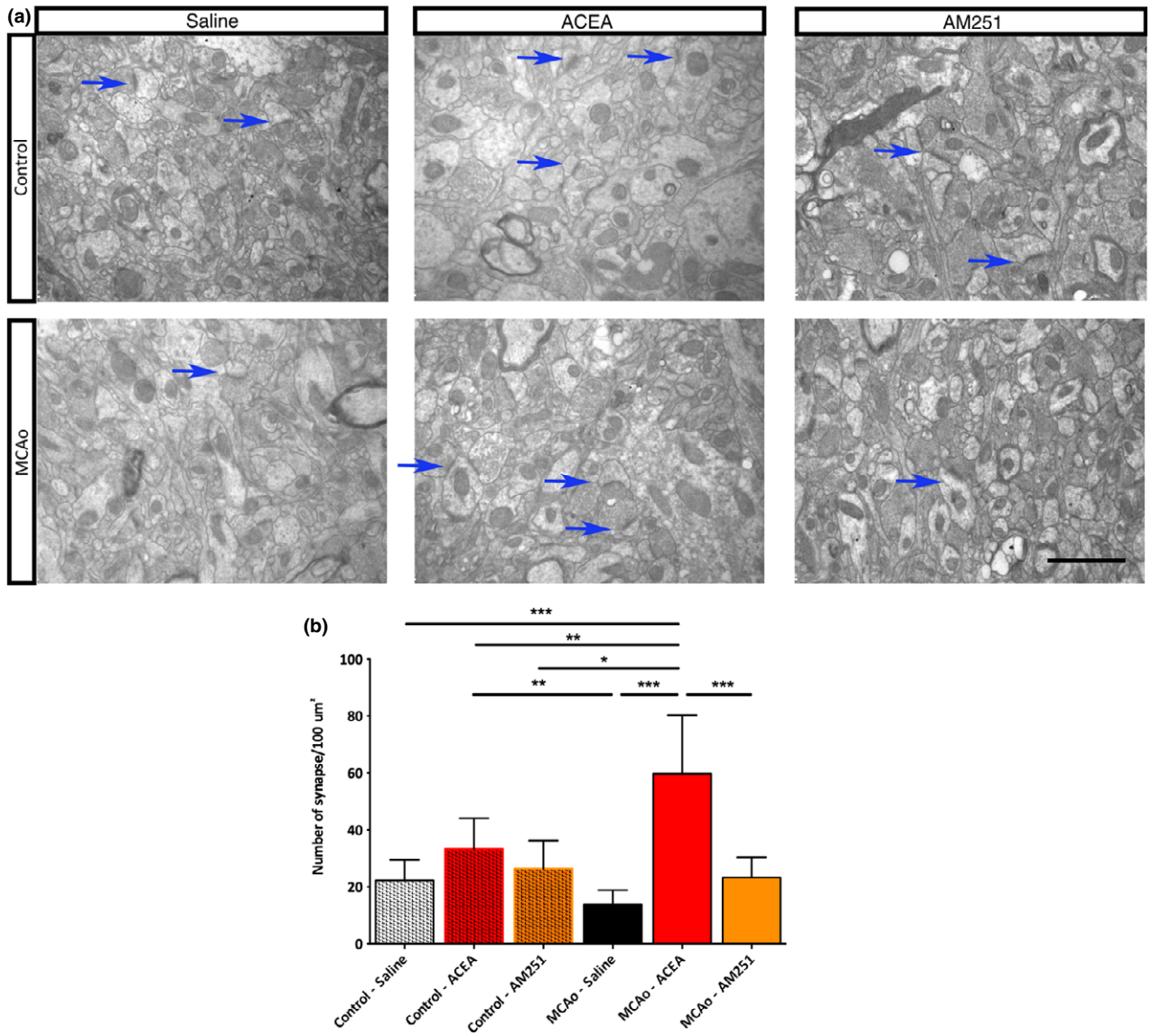

Fig. 9 (a) Transmission electron microscope (TEM) analysis. Blue arrows show synapses. (b) Number of synapses per 100 μm^2. Significance between treatments after one-way ANOVA and Tukey post-test *$p < 0.05$; **$p < 0.01$; ***$p < 0.001$. Scale bar: 2 μm.

the immune system to recruit peripheral leukocytes through systemic circulation (Macrez *et al.* 2011). MCAo produced a robust inflammatory reaction, mainly because of an increase in stellate microglial cells at D7 and with the predominance of ameboid and round lectin$^+$ microglial cells at D28. Treatment with ACEA decreased the number of microglial cells with stellate and ameboid morphology, whereas AM251 did not modify the inflammatory reaction produced by ischemia.

The neuronal degeneration, astroglial reaction and inflammatory response triggered by MCAo, as well as the recovery induced by treatment with CB1R selective agonist ACEA, might correlate with CB1R expression at D7, which is reduced in ischemic conditions – except for its selective stimulation – and demonstrates the importance of neural plasticity. CB1R has been implicated in synaptic plasticity through the coupling of post-synaptic activation with decreases in the release of pre-synaptic neurotransmitters (Alger 2014) and may play an important role in the control of neuronal circuits.

Degenerated neurons activate microglial cells, which induce normal neurons to form new synapses. This neosynaptogenesis is induced by cytokines, such as tumor necrosis factor-α, and neurotrophic factors released by activated microglia. The process named 'synaptic stripping', in which microglial cells remove pre-synaptic terminals from dendrites, allows neurons to survive and restores normal neuronal function (Trapp *et al.* 2007).

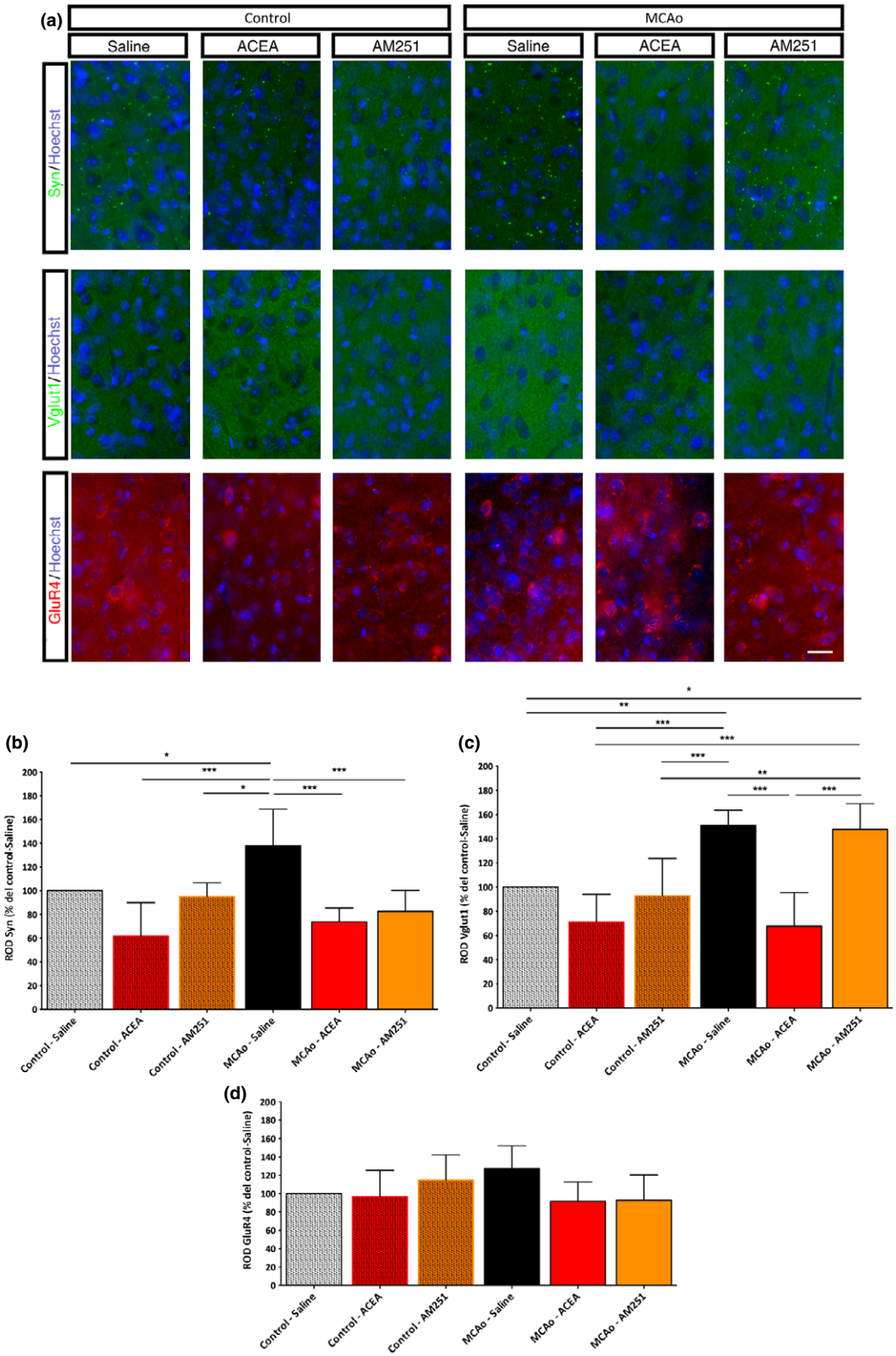

Fig. 10 (a) Syn, Vglut1 and GluR4 immunostaining. (b) Syn relative optical density (ROD). (c) Vglut1 ROD. (d) GluR4 ROD. Values are expressed as a percentage of Control-Saline group**.** Significance between treatments after one-way ANOVA and Tukey *post-test* *$p < 0.05$; **$p < 0.01$; ***$p < 0.001$. Scale bar: 30 μm.

Syn, expressed at the pre-synaptic terminal, constitutes a specific marker of pre-synaptic boutons. An increase in Syn immunoreactivity correlates with synaptogenesis, whereas its quantification is a useful tool in the estimation of synaptic density (Jung *et al.* 2009). In this study, we observed increased Syn immunoreactivity at D7 after MCAo, which correlates with levels of microglial activation. Treatment with ACEA reduced Syn immunoreactivity to normal levels, which also correlates with a reduction in microglial activation. This result is in agreement with previous studies indicating that activated microglia could exert different effects influenced by the microenvironment, thus generating beneficial or harmful impacts (Trapp *et al.* 2007). The reduction in neuronal degeneration, glutamatergic pre-synaptic vesicles and microglial activation observed in the MCAo-ACEA group, as well as the subsequent increase in the number of synapses observed by TEM at D28, could explain how CB1R agonist protects the injured area by reducing glutamate excitotoxicity and inducing new synapse formation.

Conclusions

In summary, CB1R agonist ACEA improved motor activity affected by MCAo. At histologic levels, ACEA preserved the neuronal cytoarchitecture, decreased astroglial and microglial reaction and increased synaptogenesis. Therefore, it is possible to conclude that cannabinoid agonist ACEA exerts its neuroprotective effects by acting on CB1R expression in neurons.

Acknowledgments and conflict of interest disclosure

We thank Margarita Lopez for her assistance in electron microscopy preparations. UBACYT 20020100100093BA, UBACYT 20020130100258BA (A.B.), PIP CONICET 00269 (A.B.) and UBACYT 20020130300033BA (L.C.). Authors declare no conflict of interest.

All experiments were conducted in compliance with the ARRIVE guidelines.

References

Alger B. E. (2014) Seizing an opportunity for the endocannabinoid system. *Epilepsy Curr.* **14**, 272–276.

American Heart Association Statistics Committee and Stroke Statistics Subcommittee (2014) Heart disease and stroke statistics—2014 update: a report from the American Heart Association. *Circulation* **129**, e28–e292.

Bahremand A., Nasrabady S. E., Shafaroodi H., Ghasemi M. and Dehpour A. R. (2009) Involvement of nitrergic system in the anticonvulsant effect of the cannabinoid CB(1) agonist ACEA in the pentylenetetrazole-induced seizure in mice. *Epilepsy Res.* **84**, 110–119.

Balan I. S., Fiskum G., Hazelton J., Cotto-Cumba C. and Rosenthal R. E. (2006) Oximetry-guided reoxygenation improves neurological outcome after experimental cardiac arrest. *Stroke* **37**, 3008–3013.

Caltana L., Merelli A., Lazarowski A. and Brusco A. (2009) Neuronal and glial alterations due to focal cortical hypoxia induced by direct cobalt chloride ($CoCl_2$) brain injection. *Neurotox. Res.* **15**, 348–358.

Docagne F., Muñetón V., Clemente D., Ali C., Loría F., Correa F., Hernangómez M., Mestre L., Vivien D. and Guaza C. (2007) Excitotoxicity in a chronic model of multiple sclerosis: neuroprotective effects of cannabinoids through CB1 and CB2 receptor activation Mol. *Cell. Neurosci.* **34**, 551–561.

Evrard S., Duhalde-Vega M., Tagliaferro P., Mirochnic S., Caltana L. and Brusco A. (2006) A low chronic ethanol exposure induces morphological changes in the adolescent rat brain that are not fully recovered even after a long abstinence: an immunohistochemical study. *Exp. Neurol.* **200**, 438–459.

Franklin K. and Paxinos G. (2007) *The Mouse Brain in Stereotaxic Coordinates*, pp. 25–40. 4th ed. Academic Press, San Diego.

García-Arencibia M., González S., de Lago E., Ramos J. A., Mechoulam R. and Fernández-Ruiz J. (2007) Evaluation of the neuroprotective effect of cannabinoids in a rat model of Parkinson's disease: importance of antioxidant and cannabinoid receptor-independent properties. *Brain Res.* **1134**, 162–170.

Heifets B. and Castillo P. (2009) Endocannabinoid signaling and long-term synaptic plasticity. *Annu. Rev. Physiol.* **71**, 283–306.

Jung S. H., Lee S. T., Chu K., Park J. E., Lee S. U., Han T. R. and Kim M. (2009) Cell proliferation and synaptogenesis in the cerebellum after focal cerebral ischemia. *Brain Res.* **1284**, 180–190.

Li X., Blizzard K., Zeng Z., DeVries A., Hurn P. and McCullough L. (2004) Chronic behavioral testing after focal ischemia in the mouse: functional recovery and the effects of gender. *Exp. Neurol.* **187**, 94–104.

Longa E., Weinstein P., Carlson S. and Cummins R. (1989) Reversible middle cerebral artery occlusion without craniectomy in rats. *Stroke* **20**, 84–91.

Macrez R., Ali C., Toutirais O., Le Mauff B., Defer G., Dirnagl U. and Vivien D. (2011) Stroke and the immune system: from pathophysiology to new therapeutic strategies. *Lancet Neurol.* **10**, 471–480.

Mauler F., Hinz V., Augstein K. H., Fassbender M. and Horvath E. (2003) Neuroprotective and brain edema reducing efficacy of the novel cannabinoid receptor agonist BAY 38-7271. *Brain Res.* **989**, 99–111.

Mayer M. L. (2011) Emerging models of glutamate receptor ion channel structure and function. *Structure* **19**, 1370–1380.

Pacher P. and Hasko G. (2008) Endocannabinoids and cannabinoid receptors in ischaemia-reperfusion injury and preconditioning. *Br. J. Pharmacol.* **153**, 252–262.

Parmentier-Batteur S., Jin K., Mao X., Xie L. and Greenberg D. (2002) Increased Severity of Stroke in CB1 Cannabinoid Receptor Knock-Out Mice. *J. Neurosci.* **22**, 9771–9775.

Price D. A., Martinez A. A., Seillier A. *et al.* (2009) WIN55,212-2, a cannabinoid receptor agonist, protects against nigrostriatal cell loss in the 1-methyl-4-phenyl-1,2,3,6-tetrahydropyridine mouse model of Parkinson's disease. *Eur. J. Neurosci.* **29**, 2177–2186.

Sánchez-Blázquez P., Rodríguez-Muñoz M. and Garzón J. (2014) The cannabinoid receptor 1 associates with NMDA receptors to produce glutamatergic hypofunction: implications in psychosis and schizophrenia. *Front Pharmacol.* **2**, 169.

Schallert T., Fleming S., Leasure J., Tillerson J. and Bland S. (2000) CNS plasticity and assessment of forelimb sensorimotor outcome in unilateral rat models of stroke, cortical ablation, parkinsonism and spinal cord injury. *Neuropharmacology* **39**, 777–787.

Silver R. and Curley J. P. (2013) Mast cells on the mind: new insights and opportunities. *Trends Neurosci.* **36**, 513–521.

Sofroniew M. V. and Vinters H. V. (2010) Astrocytes: biology and pathology. *Acta Neuropathol.* **119**, 7–35.

Todd A. J., Hughes D. I., Polgár E., Nagy G. G., Mackie M., Ottersen O. P. and Maxwell D. J. (2003) The expression of vesicular glutamate transporters VGLUT1 and VGLUT2 in neurochemically defined axonal populations in the rat spinal cord with emphasis on the dorsal horn. *Eur. J. Neurosci.* **17**, 13–27.

Trapp B., Wujek J., Criste G., Jalabi W., Yin X., Kidd G., Stohlman S. and Ransohoff R. (2007) Evidence for synaptic stripping by cortical microglia. *Glia* **55**, 360–368.

Vendel E. and de Lange E. C. (2014) Functions of the CB1 and CB 2 receptors in neuroprotection at the level of the blood-brain barrier. *Neuromolecular Med.* **16**, 620–642.

Wagner D., Riegelsberger U., Michalk S., Härtig W., Kranz A. and Boltze J. (2011) Cleaved caspase-3 expression after experimental stroke exhibits different phenotypes and is predominantly non-apoptotic. *Brain Res.* **1381**, 237–242.

Wang D. and Bordey A. (2008) The astrocyte odyssey. *Prog. Neurobiol.* **86**, 342–367.

Youssef F. F., Hormuzdi S. G., Irving A. J. and Frenguelli B. G. (2007) Cannabinoid modulation of neuronal function after oxygen⁄glucose deprivation in area CA1 of the rat hippocampus. *Neuropharmacology* **52**, 1327–1335.

Zani A., Braida D., Capurro V. and Sala M. (2007) D-tetrahydrocannabinol (THC) and AM 404 protect against cerebral ischaemia in gerbils through a mechanism involving cannabinoid and opioid receptors. *Br. J. Pharmacol.* **152**, 1301–1311.

Zhang L., Schallert T., Gang Zhang Z., Jiang Q., Arniego P., Li Q., Lu M. and Chopp M. (2002). A test for detecting long-term sensorimotor dysfunction in the mouse after focal cerebral ischemia. *J. Neurosci. Methods* **117**; 207–214.